

Molten-Alloy Driven Self-Assembly for Nano and Micro Scale System Integration

Ehsan Saeedi¹, Shaghayegh Abbasi¹, Karl F. Böhringer¹ and Babak A. Parviz¹

Abstract: Self-assembly is emerging as one of the main methods for construction of heterogeneous systems consisting of multiple component types in nano- and micro-scales. The engineered self-assembly used for system integration involves preparation of parts that can recognize and bind to each other or a template, and perfection of procedures that allow for high yield self-assembly of these parts into a system. Capillary forces resultant from molten alloys are attractive candidates for driving such self-assembly processes as they can simultaneously provide electrical and mechanical connections. The basic self-assembly process is reviewed here. Selection of the appropriate alloy, a critical issue in development of the self-assembly mechanism, is discussed and various candidates are identified. Examples are provided in which alloys are used to interconnect parts in nano- and micro-scales or produce three-dimensional structures. We conclude with a brief discussion of opportunities and challenges ahead in the development of system integration processes taking advantage of self-assembly.

1 Introduction

Packaging of components at the micro and nano scales is a major challenge for developing complex heterogeneous integrated systems. The most common ways used today for putting multi-component microsystems together are: pick and place robotic assembly [Hessler (1996)], microstructure transfer between aligned wafers [Cohn et al. (1998), Holmes and Saidam (1996)], and self-assembly [Parviz et al. (2005)]. Robotic assembly is a reliable method; however it is a serial process and cannot be applied in assembling very large numbers of components, especially when the size of components decreases to a few microns and smaller [Morris et al. (2005)]. Transferring microstructures between aligned wafers can handle a large number of parts; however, as the component sizes decrease maintaining the alignment accuracy becomes exceedingly difficult. In addition, wafer-level transfer is

an inherently two-dimensional (2D) fabrication method and cannot generate truly three-dimensional (3D) structures. Self-assembly, defined as the spontaneous formation of structures from a collection of interacting micro-fabricated parts, is a parallel manufacturing process that can handle a very large number of components and produce 3D structures.

The basic approach taking advantage of self-assembly involves microfabrication of freestanding/released components; functionalization of the components to allow for their participation in a self-assembly process; and development of procedures to self-assemble complete structures and systems via self-assembly. Parts that participate in a self-assembly process need to have the ability to find each other and appropriately connect to form the final structure. Mechanical interconnections hold the final structure together and the electrical connections between the components make the final self-assembled structure electrically functional. There are different ways to make the electrical connection between miniaturized components including: soldering [Dytrych (1993)], electroplating, electroless plating, and using polymers (Electrically Conductive Adhesives) [McCreery (2004), Haiss et al. (2004), Lee et al. (2004)]. Electroplating and electroless plating produce reliable electrical contacts albeit with usually poor mechanical properties [Xiong et al. (2003)]. Polymer contacts are relatively easy to fabricate and can be scaled down to sub-micron dimensions. However, their electrical resistivity is high, their contact area may be limited to asperities, and at the molecular level they may not be able to withstand high-temperature processing and operation [McCreery (2004)].

Using molten alloys (solders) to link different parts to each other or to a template can produce connections with excellent electrical and mechanical properties. In this scheme, metal pads are positioned on the components to be attached. One or both of the metal pads are covered by an alloy. In the self-assembly process, the temperature of the environment is increased to melt the alloy and the parts are allowed to randomly move. When the molten al-

¹ Department of Electrical Engineering, University of Washington, Seattle, USA

loy is in contact with both wettable metal pads it rapidly reacts to form an intermetallic compound (IMC). The resultant capillary force bonds the two parts together and a mechanical and an electrical connection between the components are made at once. After the bond formation, the temperature is lowered to solidify the molten alloy and to make the bond permanent. Soldering at larger length scales is in extensive use in the semiconductor industry for packaging and interconnection. Taking advantage of capillary forces from molten alloys in self-assembly, especially in the sub-micron length scales, is a much more recent use of the phenomenon. Our goal is to survey some of the critical issues in developing a self-assembly technology that relies on such capillary forces for systems integration. We begin our discussion in the next section by a brief description of the overall self-assembly procedure. A critical element in the process development is the selection of the appropriate alloy for interconnecting the parts. We catalogue many of the available candidates and discuss issues regarding the extension of their use to the nano-scales. We will follow by reviewing some of the recent developments in using metals and alloys for integration in nano and micron-scales. Molten-alloy driven self-assembly has not been demonstrated in the nano-scale to this date; however, some of the promising works at this length scale on forming metal interconnects to nano-scale components point toward the high potential of this approach in system integration. We review the use of molten alloys for the self-assembly of micron-scale components in the following sections. Such self-assembly schemes have been used both for interconnection of freestanding components and for moving structures to form 3D functional microstructures. After a brief review of modeling, we conclude with a discussion of challenges and opportunities ahead.

2 The Fluidic Self-Assembly (FSA) Process

System integration via FSA involves fabrication of components that have the ability to recognize and bind to each other or a template, introduction of these components in a fluid medium usually accompanied by heat and agitation, and formation of ordered structures as the entire collection of components proceeds towards a minimum energy state. After the completion of the process and formation of the structures, the energy input can be removed to make the formed structures permanent.

In the nano-scale, nanowires [Ye et al. (2006), Evoy

et al. (2004), Ye et al. (2005)] and carbon nanotubes (CNT) [Madsen et al. (2003)] have been used as components in FSA processes. These components are cheap and easy to produce; however, they offer limited functionality and complexity at the component level. The trade-off between component size and complexity is one that is prevalent in dividing the nano and micro domains. In general, nano-scale elements offer a size advantage but provide less functionality compared to micron-scale components. For example, a microfabricated micron-scale element can readily incorporate a circuit with tens of transistors and have a specific geometry to allow for selective self-assembly based on complementary shape recognition [Stauth and Parviz (2005) a, Stauth and Parviz (2005) b]. Such a component can be made via surface and bulk micromachining methods followed by release steps [Talgader et al. (1995)]. Currently, methods to generate nano-scale components with a comparable level of complexity do not exist.

A number of forces have been employed to control the interaction between parts in a FSA procedure and to agitate and guide the structures towards their minimum energy state. They include forces related to gravity [Stauth and Parviz (2005) a, Stauth and Parviz (2005) b], electric field [Tu et al. (2003)], magnetic field [Ye et al. (2006), Ziegler and Srinivasan (1996)], and surface tension [Jacobs et al. (2002), Gracias et al. (2000)]. Gravitational forces scale unfavorably to smaller dimensions. These forces can be used to guide components in the micron-scale [Talgader et al. (1995)]; however their ability to overcome other forces steadily diminishes as the size scale of the components is reduced to a micron and smaller. Other forces, such as ones resultant from application of electric and magnetic fields, are used to guide the self-assembly of nano-scale components such as nanowires; however, they do not generate permanent bonds between the components. When surface tension is used as the driving force in self-assembly, materials with specific melting points are positioned on the binding sites on the components or the template. The components are submerged in a fluid medium and the temperature is raised to melt the material positioned on the binding sites. When two sets of molten zones meet, surface energy minimization forms a bond between the two. Polymers [Syms (1999), Syms (2001) a], glass [Syms (1998), Syms et al. (1996)], and solders [Jacobs et al. (2002), Gracias et al. (2000)] have been used to generate

capillary forces in FSA processes. A major advantage offered by molten-alloys or solder is the ability to form both mechanical and electrical connections at once.

Selection of the material to form the capillary bond on the interconnect pads is a critical issue in designing a self-assembly process. Tin-lead alloys have been the most widely used materials in molten-alloy driven self-assembly; however, since alloys containing lead are scheduled to be phased out of industrial production in near future alternative materials are needed as substitutes for these alloys. Electrically conductive adhesives (ECAs) require mild processing conditions, exert low stress levels on the substrate, and can be patterned as fine pitch interconnects. However, their low electrical conductivity, early electrical fatigue, and poor impact strength [Li and Wong (2006)] are impeding factors in their implementation in system integration applications. The most viable candidates in near future are lead-free alloys. In the following section we discuss various alloys available and the issues involved in their implementation for generation of capillary forces and making mechanical and electrical connections in the sub-micron regime.

3 Selecting Alloys For Fluidic Self-Assembly

Solder alloys with various characteristics are in extensive use in the semiconductor industry today to form electrical connections between chips and their packages. The typical size of the solder bumps in state-of-the-art packaging is $100\ \mu\text{m}$ with an equal pitch yielding near 2500 Input/Output interconnects on a $1\ \text{cm}^2$ chip. Fig. 1 shows an example of such solder bumps [Tu et al. (2003)].

Alloys containing lead have been traditionally used to form connections however, as mentioned above, their use will be restricted in the near future due to environmental concerns. Another disadvantage of using Pb on Si chips is the existence of an isotope of Pb that emits alpha particles and decays to Bi. This alpha emission can generate electron-hole pairs in Si which causes soft errors, especially in capacitors (memory units) [Ziegler and Srinivasan (1996)]. Extensive development efforts are underway to find a proper substitute for lead-containing alloys. These efforts can also help in identifying suitable alloys for self-assembly. Tab.1 shows the melting point temperature and other properties of various alloys available for self-assembly.

An important issue when molten alloys are used for form-

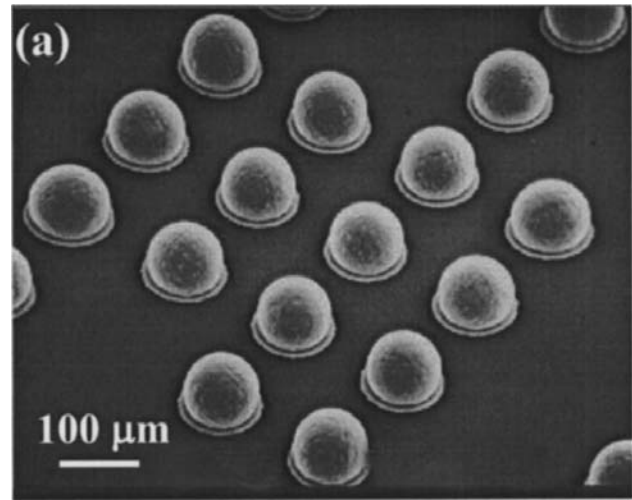


Figure 1 : Area array of solder balls on a Si chip surface [Tu et al. (2003)].

ing connections is the inter-diffusion of the metal pads and the molten alloy and formation of inter-metallic compounds (IMC). The formation of IMC can significantly impact the mechanical and electrical characteristics of the interconnect, change the surface tension forces, and even change the chemical properties of the alloy in the fluidic self-assembly environment. For example, experiments show that during wetting reactions, a tin-based molten solder can consume a $1\ \mu\text{m}$ thick Cu film in less than 1 min [Tu et al. (2003)]. The interfacial reaction between the solder and Cu forms IMCs of Cu_6Sn_5 [Kim et al. (1995), Kim and Tu (1996), Erinc et al. (2004)]. The Au/Sn system exhibits interdiffusion and produces the phases AuSn , AuSn_2 , and AuSn_4 at room temperature with the 0.05Au-0.95Sn having the lowest eutectic temperature ($217\ ^\circ\text{C}$) of the Au-Sn system [Ishii and Aoyama (2004)]. The formation of IMC, containing ionic and covalent bonds, can lead to abrupt changes in mechanical properties of the material [Harsh et al. (2000)]. Also, the rapid rate of consumption of the metal pads may limit the time-scale of the self-assembly process. For sub-micron elements containing metal pads that are only a few tens of nanometers thick, the rapid dissolution of the pad metals into the molten alloy presents a major obstacle in forming bonds.

Many lead-free alloys used for forming electrical connections are tin-based. A special class, the eutectic alloys of Sn with coinage metals such as Au, Ag, and Cu

Table 1 : Candidate metal alloys and their properties

Alloy	Melting Temp. (°C)	Surface Energy Surface Tension T (°C) (N/m)		Oxide Thickness (Angstrom)	Ref.
Sn-37 Pb	183*	0.417 ^a			[Abtew and Selvaduray (2000)], [Syms et al. (2003)]
Sn-40Pb	187 ⁺			35	[Abtew and Selvaduray (2000)], [Kuhmann et al. (1998)]
Bi-26In-17Sn	79				[Abtew and Selvaduray (2000)]
Bi-32In	109.5*				[Abtew and Selvaduray (2000)]
Bi-41.7Sn-1.3Zn	127				[Abtew and Selvaduray (2000)]
Bi-42Sn		0.319 ^a			[Abtew and Selvaduray (2000)]
Bi-43Sn (eutectic)	139*				[Abtew and Selvaduray (2000)]
Bi-43Sn+2.5%Fe	139*				[Abtew and Selvaduray (2000)]
Bi-45Sn-0.33Ag	140-145				[Abtew and Selvaduray (2000)]
In-3Ag	141*				[Abtew and Selvaduray (2000)]
In-34Bi	110*				[Abtew and Selvaduray (2000)]
In-48Sn (eutectic)	117*			After 50 min: 60 T=100 °C After 50 min: 500 T=150 °C	[Abtew and Selvaduray (2000)], [Kuhmann et al. (1998)]
Sn-1Ag-1Sb	232 ⁺				[Abtew and Selvaduray (2000)]
Sn-2.5Ag-0.8Cu-0.5Sb	210-216	0.51			[Abtew and Selvaduray (2000)]
Sn-2.8Ag-20In	178	0.39			[Abtew and Selvaduray (2000)], [Artaki et al. (1995)]
Sn-25Ag-10Sb	233				[Abtew and Selvaduray (2000)]
Sn-2Ag	225				[Abtew and Selvaduray (2000)]
Sn-2Ag-0.8Cu-0.6Sb	210-216				[Abtew and Selvaduray (2000)]
Sn-2Ag-0.8Cu-6Zn	217 ⁺				[Abtew and Selvaduray (2000)]
Sn-2Ag-0.8Cu-8Zn	215 ⁺				[Abtew and Selvaduray (2000)]
Sn-3.5Ag	221*	0.431 ^a	271	Initial: 30 After 10 min.: 50 After 50 min.: 50 T=361 °C, Sn-oxide	[Syms et al. (2003)], [Miric and Grus (1998)]
Sn-3.5Ag-(<6)Bi	212 ⁺	0.42			[Abtew and Selvaduray (2000)], [Artaki et al. (1995)]
Sn-3.5Ag-1Zn	217				[Abtew and Selvaduray (2000)]
Sn-3.5Ag-1Zn-0.5Cu	216, 217				[Abtew and Selvaduray (2000)]
Sn-3.6Ag-1.5Cu	225				[Abtew and Selvaduray (2000)]
Sn-4.7Ag-1.7Cu	217				[Abtew and Selvaduray (2000)]
Sn-4Ag	225 ⁺				[Abtew and Selvaduray (2000)]
Sn-4Ag-7Sb	230 ⁺				[Abtew and Selvaduray (2000)]
Sn-10Au	217*				[Tu et al. (2003)]
Sn-0.58Bi		0.319 ^a	188		[Syms et al. (2003)]
Sn-10Bi-0.8Cu	217 ⁺				[Abtew and Selvaduray (2000)]

Sn-10Bi-5Sb	232 ⁺				[Abtew and Selvaduray (2000)]
Sn-42Bi	170 ⁺				[Abtew and Selvaduray (2000)]
Sn-58Bi	139*	0.349 ^N	Peak reflow temp.	Initial: - After 10 min.: 350 After 50 min.: 800 T=278 °C, Sn-oxide	[Miric and Grus (1998)], [Tu et al. (2003)], [Hua et al. (1998)]
Sn-45Bi-3Sb	178 ⁺				[Abtew and Selvaduray (2000)]
Sn-56Bi-1Ag	136.5				[Abtew and Selvaduray (2000)]
Sn-57Bi-1.3Zn	127				[Abtew and Selvaduray (2000)]
Sn-7.5Bi-2Ag-0.5Cu	212 ⁺				[Abtew and Selvaduray (2000)]
Sn-0.75Cu	229 ⁺				[Abtew and Selvaduray (2000)]
Sn-0.7Cu (eutectic)	227*	0.491 ^a	277	Initial: 20 After 10 min.: 50 After 50 min.: 50 T=367 °C, Sn-oxide	[Syms et al. (2003)], [Miric and Grus (1998)]
Sn-2Cu-0.8Sb-0.2Ag	266-268				[Abtew and Selvaduray (2000)]
Sn-3Cu	275 ⁺				[Abtew and Selvaduray (2000)]
Sn-4Cu-0.5Ag	222 ⁺				[Abtew and Selvaduray (2000)]
Sn-10In-1Ag-(0-10.5)Bi	188-197				[Abtew and Selvaduray (2000)]
Sn-20In-2.8Ag	178-189				[Abtew and Selvaduray (2000)]
Sn-42In	140 ⁺				[Abtew and Selvaduray (2000)]
Sn-10In-1Ag-0.5Sb	196-206				[Abtew and Selvaduray (2000)]
Sn-36In	165 ⁺				[Abtew and Selvaduray (2000)]
Sn-50In	125 ⁺				[Abtew and Selvaduray (2000)]
Sn-51In	120*				[Tu et al. (2003)]
Sn-52In	118			Initial: 20 After 10 min.: 175 After 50 min.: 600 T=257 °C, In-oxide	[Miric and Grus (1998)]
Sn-8.8In-7.6Zn	181-187				[Abtew and Selvaduray (2000)]
Sn-2Mg (eutectic)	200*				[Abtew and Selvaduray (2000)]
Sn-20Pb		0.503 ^f	350		[Syms et al. (2003)]
Sn-37Pb	183	0.464 ^N	Peak reflow temp.	Initial: 30 After 10 min.: 50 After 50 min.: 500 T=323 °C, Sn-oxide	[Miric and Grus (1998)], [Hua et al. (1998)]
Sn-40Pb (near eutectic)		0.417 ^a			[Abtew and Selvaduray (2000)]

Sn-40Pb		0.482 ^l	350		[Syms et al. (2003)]
Sn-60Pb		0.466 ^l	350		[Syms et al. (2003)]
Sn-80Pb		0.454 ^l	350		[Syms et al. (2003)]
Sn-5Sb	240 ⁺	0.468 ^a	290	Initial: 20 After 10 min.: 875 After 50 min.: 1425 T=380 °C, Sn-oxide	[Abteew and Selvaduray (2000)], [Miric and Grus (1998)]
Sn-4Sb-8Zn	198-204				[Abteew and Selvaduray (2000)]
Sn-7Zn-10In-2Sb	181				[Abteew and Selvaduray (2000)]
Sn-8Zn-10In-2Bi	175				[Abteew and Selvaduray (2000)]
Sn-8Zn-5In-(0.1-0.5)Ag	187				[Abteew and Selvaduray (2000)]
Sn-9Zn	199	0.518 ^a	249	Initial: 70 After 10 min.: 200 After 50 min.: 325 T=369 °C, Zn-oxide	[Syms et al. (2003)], [Miric and Grus (1998)]
Sn-9Zn-10In	178				[Abteew and Selvaduray (2000)]
Sn-5.5Zn-4.5In-3.5Bi	185-188				[Abteew and Selvaduray (2000)]
Sn-6Zn-6Bi	127				[Abteew and Selvaduray (2000)]
Sn-9Zn (eutectic)	198*				[Abteew and Selvaduray (2000)]
Sn-9Zn-5In	188				[Abteew and Selvaduray (2000)]

* Eutectic Temperature

+ Liquid Temperature

^a In air

^l In inert atmosphere

^N In nitrogen

has been extensively investigated. In this class, 95.5Sn-4.0Ag-0.5Cu is considered a particularly attractive candidate [Erinc et al. (2004), Seeling and Suraski (2001)]. Note that contamination of the solder with lead may result in nonuniformity, formation of voids and a decrease in reliability [Seeling and Suraski (2001)]. The migration of technology to the new alloys does entail an increase in cost as seen by comparing the prices: Sn-4Ag-0.5Cu US\$ 10.12, Sn-2.5Ag-0.7Cu-0.5Sb US\$7.88, Sn-36Pb-2Ag US\$ 5.92, and Sn-63Pb US\$ 2.95 [Seeling and Suraski (2001)].

Another critical issue in using metal alloys for forming

contacts is the surface oxide. The metal oxide forming on the surface of alloys can severely hamper their capacity to form capillary bonds to metal pads and conduct electricity [de kluzenaar (1983)]. To form reliable bonds, this surface oxide is usually dissolved in an acid (flux) to allow the exposure of fresh alloy surface immediately before the bond formation. In designing a self-assembly process one needs to ensure that the acid exposure does not adversely affect the components. Under ambient conditions the thickness of the native oxide on Sn/Pb, In/Sn and Au/Sn alloys is near 3.5 nm [Kuhmann et al. (1998)] immediately setting a lower limit on the thickness of alloy films used in self-assembly. The formation of the

crystalline oxide layer is self-limiting at room temperature. As mentioned above, the self-assembly process is conducted in a heated environment with molten alloys. At elevated temperatures, the oxide thickness can rapidly increase. Fig. 2 shows the evolution of the thickness of the oxide layer on an In/Sn alloy at high temperature in vacuum and ambient O_2 pressures [Kuhmann et al. (1998)]. The oxidation of the alloy reduces the volume of metal that can be used in forming capillary bonds (since the oxide must be dissolved away before a metal bond can be formed). This loss of material is particularly severe in nano-scale applications and can essentially exclude the use of alloys for making contacts between nano-scale components. To avoid a high rate of oxidation the partial pressure of oxygen should be reduced or inert gasses used in the self-assembly process chamber. Oxide thickness of different alloys is catalogued in Tab.1.

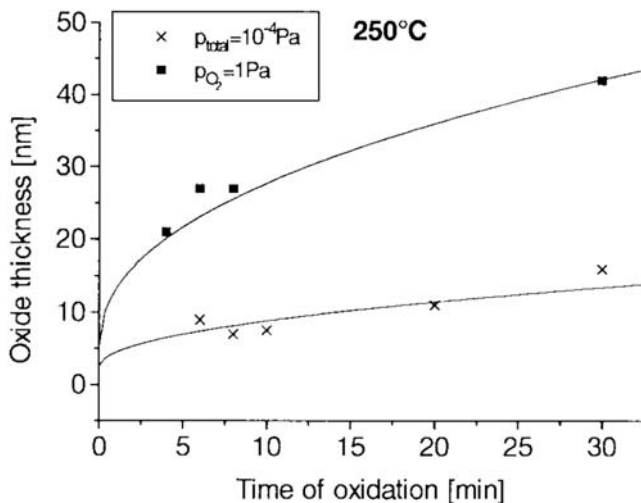


Figure 2 : Oxide growth on eutectic In/Sn with different O_2 partial pressures at 250 °C [Kuhmann et al. (1998)].

Electromigration is another limiting factor in scaling down contacts made from alloys. The small size of contacts results in a high current density and hence fast atomic diffusivity in solder alloys [Huynh et al. (2001), Xu (2001)]. The high current density results in movement of voids in the alloy toward the cathode and can induce very large compositional redistributions [Nah et al. (2006), Yeh et al. (2002)]. Heat generated because of current flow can induce non-uniform expansion and extra mechanical stress in the structure. In a structure self-assembled using molten-alloy capillary bonds, the alloys are not only responsible for forming electrical con-

nections but they also provide the mechanical bonds and must ensure the mechanical integrity of the final structure. Depending on the application, the final structure may be subjected to varied levels of mechanical stress. Tab.2 catalogues the mechanical properties of candidate alloys to help in choosing a suitable one for a specific application.

4 Wetting and Mechanisms of Bond Formation by Solder

When a molten solder volume touches a metal pad, a number of different physical and chemical phenomena proceed simultaneously until a static contact angle is formed and the system reaches the equilibrium state. Surface tension imbalance, viscous dissipation, molecular kinetic motion, chemical reaction, and diffusion are just a few parameters that must be taken into account for the thorough analysis of the complex process of wetting and bond formation [Kang et al. (2005)]. A number of analyses of the wetting process have been performed by focusing on one of the phenomena listed above and neglecting the others. Examples of such analyses include: simulations done using surface evolver based on the static surface tension model [Renken and Subbarayan (1998)], calculations based on energetic and kinetics of the dissolutive wetting process performed under the assumption that substrate dissolution controls the wetting kinetics [Yost et al. (1998)], modeling of the solder profile evolution and triple point line motion driven by surface tensions and the gravity field assuming that the velocity of the interface (wetting kinetics) is a linear function of the driving force [Gao et al. (2000)], and wetting analysis performed using de Gennes's model [de Gennes (1985)] assuming there is no interaction or coupling other than van der Waals forces between the liquid and solid phases. Despite varied degrees of success, empirical observations show that none of these models can fully explain the behavior of molten solder during reactive wetting [Kang et al. (2005), Whalley and Conway (1996)]. The experimental observations indicate that the wetting dynamics clearly depend on temperature, solder materials, and the substrate metallization. Fig. 3 [Kang et al. (2005)] shows the dependence of the contact angle evolution over time on temperature for eutectic Pb-Sn solder on Cu/Ni/Au substrate. The rate of many processes contributing to the solder bond formation increase with temperature such as the reactivity between solder and substrate material and

Table 2 : Mechanical Properties of candidate alloys

Alloy	Elastic Modulus (GPa)	Yield Strength (MPa)	Ultimate Tensile Strength (MPa)	Percent Elongation	Ref.
Sn-37Pb	39, 30.5	27.23	19 at 20 °C, 4 at 100 °C	48%	[Abteu and Selvaduray (2000)], [Technical Reports (1998)]
Sn-75Pb		23.62		53%	[Technical Reports (1998)]
Bi-41Sn-1Ag				40% at 25 °C	[Abteu and Selvaduray (2000)]
Bi-41Sn-1Pb			73 at 0.4/s strain rate, cast processing 55 at unspecified strain rate and processing 71 at unspecified strain rate and bulk processing		[Abteu and Selvaduray (2000)]
Bi-42Sn	42	41		73-150% at strain rate 0.005<X<0.0033 4.9% at -65 °C, 20% at 25 °C, 159% at 85 °C	[Abteu and Selvaduray (2000)]
In-48Sn (eutectic)	23.6, 19.5				[Abteu and Selvaduray (2000)]
Sn-2Ag-9.8Bi-9.8In		100.39		7%	[Technical Reports (1998)]
Sn-2Ag-7.5Bi-0.5Cu		85.29			[Technical Reports (1998)]
Sn-2.5Ag-19.5Bi		83.22			[Technical Reports (1998)]
Sn-3Ag-54Bi-2Cu-2Sb		78.88		4%	[Technical Reports (1998)]
Sn-2.5Ag-0.8Cu-0.5Sb	29.4	22.83	39.5	42.4%	[Abteu and Selvaduray (2000)], [Technical Reports (1998)]

Sn-3.5Ag	50	48	42.8 at 5 °C/min cooling 55 at 0.022 strain rate, cast Processing 37 at 0.000033 strain rate, cast processing 20 at 0.00015 strain rate, cast, aged 25 °C 56 at 0.0008 strain rate, cold rolled sheet 37 at 20 °C		[Abtew and Selvaduray (2000)]
Sn-5Ag	34				[Abtew and Selvaduray (2000)]
Sn-3.5Ag-<6Bi			71.7 at 5 °C/min cooling	15% at 5 °C/min cooling 40% at 0.00015/s strain rate 25% at 0.033/s strain rate 31% at 0.000033/s strain rate	[Abtew and Selvaduray (2000)]
Sn-3.5Ag-1Zn			52.2 at 5 °C/min cooling	27.5% at 5 °C/min cooling	[Abtew and Selvaduray (2000)]
Sn-3.5Ag-1Zn-0.5Cu			48.3 at 5 °C/min cooling	7% at 5 °C/min cooling	[Abtew and Selvaduray (2000)]
Sn-42Bi				16.6%	[Abtew and Selvaduray (2000)]
Sn-31.5Bi-3Zn		72.39		53%	[Technical Reports (1998)]
Sn-5Bi-3.5Ag			71.7 at 5 °C/min cooling	15% at 5 °C/min cooling	[Abtew and Selvaduray (2000)]
Sn-56Bi-2In				116%	[Technical Reports (1998)]
Sn-20In-2.8Ag	38.6 at 20 °C		46.9 at unspecified cooling rate	47% at unspecified cooling rate	[Abtew and Selvaduray (2000)]
Sn-30In		17			[Abtew and Selvaduray (2000)]
Sn-42In				38% at 5/s strain rate	[Abtew and Selvaduray (2000)]

Sn-60In		4.5			[Abtey and Selvaduray (2000)]
Sn-5In-3.5Ag			62.1 at 5 °C/min cooling	20% at 5 °C/min cooling	[Abtey and Selvaduray (2000)]
Sn-8Zn-4In			50.3 at 5 °C/min cooling	25% at 5 °C/min cooling	[Abtey and Selvaduray (2000)]
Sn-8Zn-5In(0.1-0.5)Ag			52.4 at 5 °C/min cooling rate (0.1%Ag)	40% at 58C/min cooling rate (0.1% Ag)	[Abtey and Selvaduray (2000)]
Sn-9Zn-10In			52.2		[Abtey and Selvaduray (2000)]
Sn-9Zn (eutectic)			64.8 at 5 °C/min cooling rate, 103	45% at 5 °C/min cooling rate	[Abtey and Selvaduray (2000)]
Sn-9Zn-5In			62.1		[Abtey and Selvaduray (2000)]
Sn-5Sb		25.65	31 at 20 °C 20 at 100 °C	25% at 20 °C 31% at 100 °C	[Abtey and Selvaduray (2000)]

the diffusion of reactants in the solder alloy. On the other hand the viscosity of molten solder and its surface tension decrease with temperature allowing for higher mobility of the solder volume at elevated temperatures.

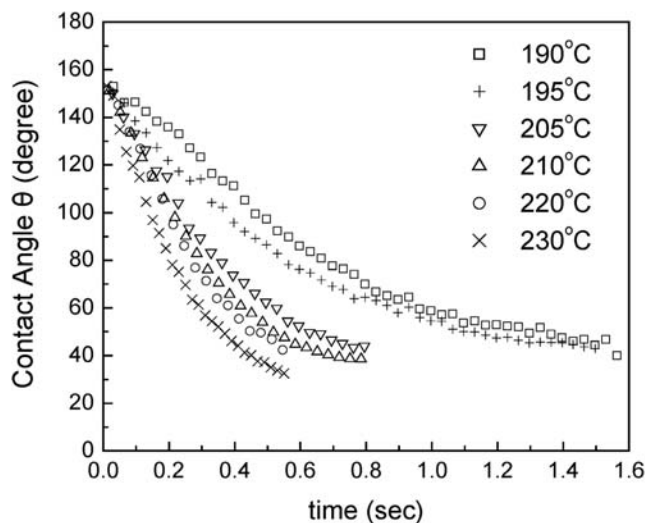


Figure 3 : Variations of contact angle over time for a eutectic tin–lead solder on a Cu/Ni/Au substrate at six temperatures [Kang et al. (2005)].

Different metal pads have different rates of reaction and IMC formation with solders, which can affect the wetting process. For example Cu reaction with Sn is faster than

Ni, and Au dissolves very fast in tin-based solders [Bader (1969)]. Consequently, tin-rich solder reaches the equilibrium contact angle faster on Cu than Cu/Ni/Au, with just a thin layer of gold (since the gold layer is very thin, Ni is dominant in specifying the IMC formation rate) [Kang et al. (2005)]. Fig. 4 shows how the eutectic Sn-Pb solder evolves as it contacts a Cu/Ni/Au substrate and wets the surface. In this case the diffusion and reaction kinetics of the Sn and substrate metallization tend to govern the wetting dynamics. It has been reported that a small increment in the percentage of Sn in high-Pb Sn-Pb solder significantly improves the wettability of Pb-xSn solder on Cu [Wang et al. (2006)]. Despite significant efforts in the area, a comprehensive understanding of the solder bond formation processes is yet to emerge.

5 Self-Assembly and Forming Metal Contacts in Nano-Scale

Forming good electrical contacts to nano-scale components is one of the major challenges faced for integration of these components into systems. Molten-alloy driven self-assembly has not been demonstrated to this date for system integration at the nano-scale. However a few pioneering works in forming metal contacts to nano-scale components, as briefly surveyed below, point towards the high potential of this approach. It is interesting to note that the melting point decreases with the decreased size

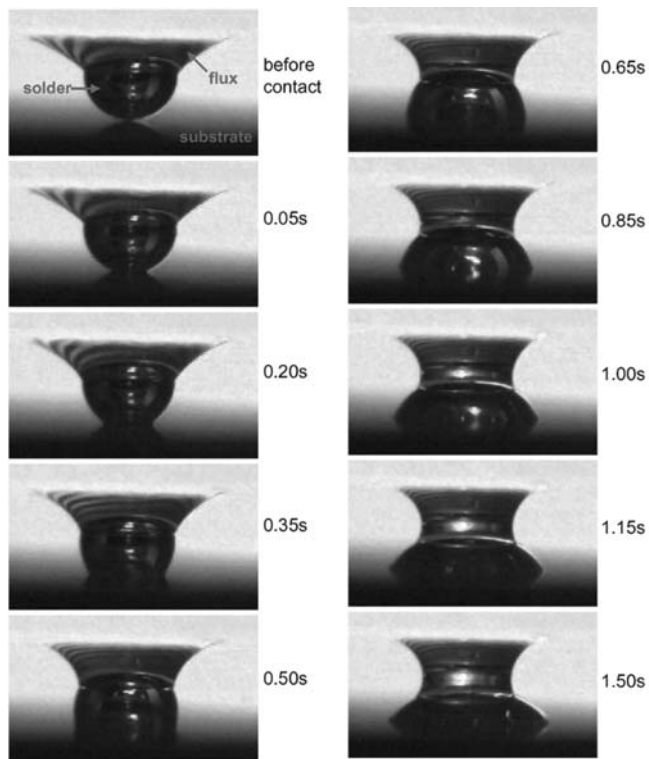


Figure 4 : Images of a eutectic tin–lead solder on a Cu/Ni/Au substrate, where the diameter of solder sphere is 635 μm , and the ambient temperature is 190 C at various wetting times [Kang et al. (2005)]

of the structure [Unruh et al. (1993)]. This observation is in good agreement with the results of a classical thermodynamic treatment of melting in finite systems and may enable forming metal contacts to temperature sensitive structures and materials that are incompatible with the procedure in larger scales.

5.1 “Soldering” to carbon nanotubes

Unique electrical and mechanical properties of carbon nanotubes have made them attractive candidates as nano-scale building blocks for forming integrated systems [Collins and Avouris (2000)]. It has been shown that two-thirds of all possible single-walled nanotubes are one-dimensional semiconductors, whereas the remaining one-thirds are one-dimensional metals [Saito et al. (1992), Wilder et al. (1998), Odom et al. (1998)]. Unmodified crossed single-wall metallic nanotube junctions show a very high resistance of approximately 200 k Ω [Fuhrer et al. (2000)], which is partly due to the small contact area of about 1 nm². Metals can increase the con-

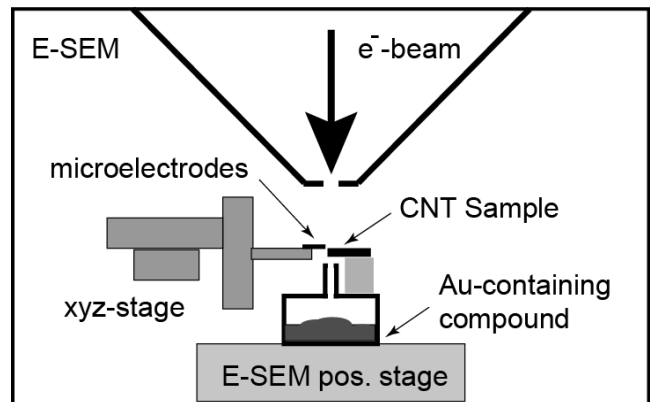


Figure 5 : Setup for positioning and soldering of carbon nanotubes onto microelectrodes inside an E-SEM [Madsen et al. (2003)].

tact area and enable the formation of low resistance interconnects between carbon nanotubes and a larger structure. Nano-scale “soldering” have been demonstrated for connecting nanotubes to gold microelectrodes.

Here is an example of metal contact formation between carbon nanotubes and adjustable gold cantilevers at the nano-scale. Free standing multi-wall carbon nanotubes (MWNT) with diameters between 50-120 nm were grown on a silicon substrate using chemical vapor deposition [Madsen et al. (2003)]. Some carbon nanotubes would extend over the edge of silicon substrate, which made them accessible for contact formation on gold electrodes. Microcantilever gold electrodes extending over the edge of a silicon chip were fabricated using standard microfabrication methods. To form the contacts, the microelectrode chip was mounted on a translation stage with xyz position control inside an environmental scanning electron microscope (E-SEM). The MWNT sample was placed close to the opening of a gold-compound source (Dimethylacetylacetonate gold (III)), which was mounted on the position stage of the E-SEM (Fig. 5).

Next, the electron-beam was slowly scanned across the nanotube at the point of contact with the electrodes. The electron-beam assisted deposition of gold from the organo-metallic precursor made a metal junction between the MWNT and the electrode effectively soldering the two (Fig. 6). Resistance measurement of four different nanotubes after completion of soldering showed 9 k Ω , 11 k Ω , 27 k Ω , and 29 k Ω , which remained constant

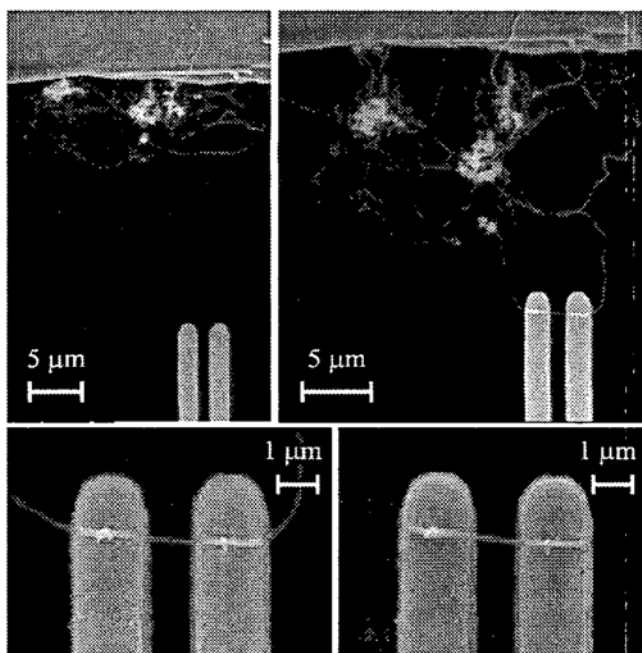


Figure 6 : Positioning, soldering and release of a carbon nanotube bridge device. A microelectrode pair was positioned so that a nanotube bridged the gap. Electron-beam assisted deposition of gold soldered the nanotube at both ends to the electrode (upper panel). A higher beam current at the outer edge of the electrodes can be used to release the device. The lower panel shows the device before (left) and after (right) release from the nanotube extensions [Madsen et al. (2003)].

over time in air. A control experiment involving the deposition of carbonaceous material originating from the background gas in a high vacuum SEM showed contact resistance in the $M\Omega$ range verifying the effectiveness of the nano-scale soldering method.

5.2 Forming contacts to metallic nanowires

There are two major challenges in the self-assembly of nanowires: precise positioning, and forming low resistance electrical contacts. A common way of positioning which can be used on nanowires with ferromagnetic nickel segments is magnetic directing [Tanase et al. (2002)]. In [Ye et al. (2005)] both magnetic positioning and soldering of metal nanowires have been reported. To prepare a template for self-assembly, contact micro-pads were fabricated using standard fabrication methods. The pads were made of Cr (adhesion promoter), Ni (magnetic), Cu (readily wettable by alloy), and Sn/Pb alloy.

Next Au-Ni nanowires with diameter of 50-200 nm were positioned and magnetically directed on the pads (Fig. 7). To perform this step, the substrate patterned with the contact pads was placed at the bottom of a vial, and a few drops of a suspension of nanowires in ethanol was placed on its surface. The concentration of wires in the suspension was estimated at approximately 10 wires/ml. The vial was then placed in a magnetic field (200 G) for 20 to 30 min causing the alignment of the nanowires between contact pads. The nanowires were permanently attached to the contact pads using alloy reflow. Reflow was done in nitrogen environment to prevent excessive oxidation of alloy—a critical issue in nano-scale soldering. The reflow temperature was kept below $220\text{ }^{\circ}\text{C}$ to reduce the rate of intermetallic compound formation. After reflow, samples were cooled slowly to form reliable solder connections [Ye et al. (2006)]. The electrical resistance of the nanowire bridged contact pads before reflow ranged between $300\ \Omega$ to $10^6\ \Omega$. After reflow, the contact resistance decreased substantially to $10\ \Omega$ to $50\ \Omega$.

5.3 Soldering silver nanoparticles

Metal or semiconductor nanoparticles can also be used as building blocks in nano-scale integrated structures [Colvin et al. (1994)]. It is possible to fuse silver nanoparticles (20 nm to 35 nm) positioned near each other to form a larger structure [Mallicka et al. (2005)]. Silver nanochains can be obtained by putting silver nanoparticles in an oriented polymer such as methoxy polyethylene glycol (MPEG). Upon ultraviolet irradiation MPEG generates free radicals that serve as the reducing agent for silver ions, causing them to link the nanoparticles. Dependent on the concentration of silver ions in solution and the density of nanoparticles, the resulting structure may be a single chain (low concentration) or a cross-linked nanochain (high concentration) (Fig. 8).

The above examples show that metal contacts can be formed to nano-scale objects. Besides heat, electron beams and photon irradiation may be used to initiate nano-scale soldering of these objects. The results reviewed here are promising and pave the way for the development of a self-assembly process taking advantage of alloys. The large forces resultant from metallic bonds are expected to hold structures made via molten-alloy driven self-assembly firmly together at the nano-scale. We now turn our attention to molten-alloy driven self-

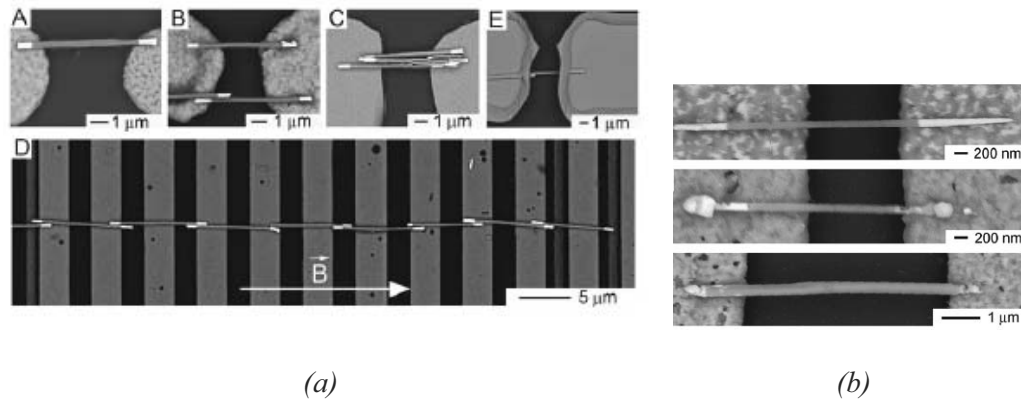


Figure 7 : (a) Directed assembly of nanowires on top of patterned substrates using magnetic fields. The wires align between the pads in the direction of the field. Number of wires between pads is determined by the concentration of the wire suspension (b) Nanosolder reflow results with slow cooling [Ye et al. (2006)].

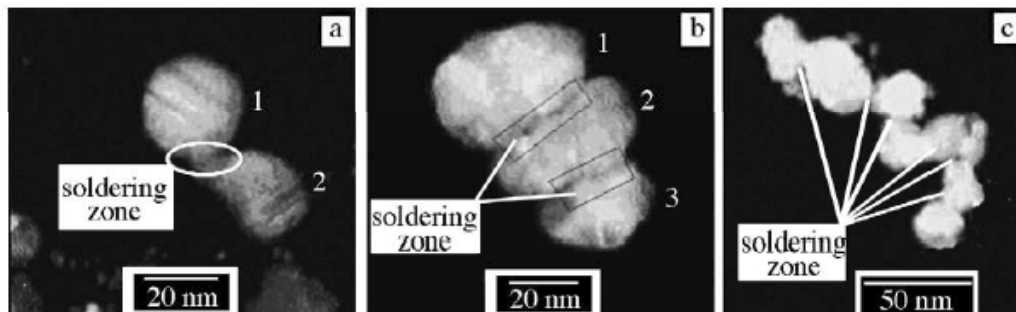


Figure 8 : Transmission Electron Microscope (TEM) images of silver chains containing different numbers of silver nanoparticles. The image shows the 'soldering zones' where assembly of the nanoparticles takes place to form a nanochain. (a) Two soldered particles, (b) three particles soldered together, (c) seven soldered silver particles [Mallicka et al. (2005)].

assembly in the micron-scale. This area has witnessed rapid progress in the recent years.

6 Molten-Alloy Driven 2D Self-Assembly in Micro-Scale

Capillary forces resultant from molten metals and alloys can be used to integrate microfabricated components into 2D templates for construction of heterogeneous integrated systems. An early application of this approach for integration of compound semiconductor components on silicon substrates was reported in [Talgader et al. (1995)]. In this work, a 700 nm layer of tin was patterned on a silicon template and a thick gold pattern was positioned on released $40 \mu\text{m} \times 40 \mu\text{m}$ light emitting diodes (LED) to be assembled on the template. During the self-assembly process, the LEDs were trapped in the binding sites on the template with matching shapes, putting the

gold pads adjacent to the tin layer on the template. Heating the template to 232°C , near the melting point of Sn, caused the diffusion of Sn into gold and forming a good mechanical and electrical contact between the LEDs and the template. This processes demonstrated yields approaching 90% for FAS.

Molten-alloy driven self-assembly of $300 \mu\text{m}$ LEDs on plastic substrates has also been reported [Jacobs et al. (2002), Zheng et al. (2005) a, Zheng and Jacobs (2005) b]. Here, alloy-coated areas acted both as receptors for the components during self-assembly and as electrical connections during operation. To form the structure, a plastic template containing binding sites coated with a low melting point alloy was prepared. A collection of LEDs with gold contacts on both sides were introduced on the template submerged in a heated fluid. Energy minimization between the components and the template re-

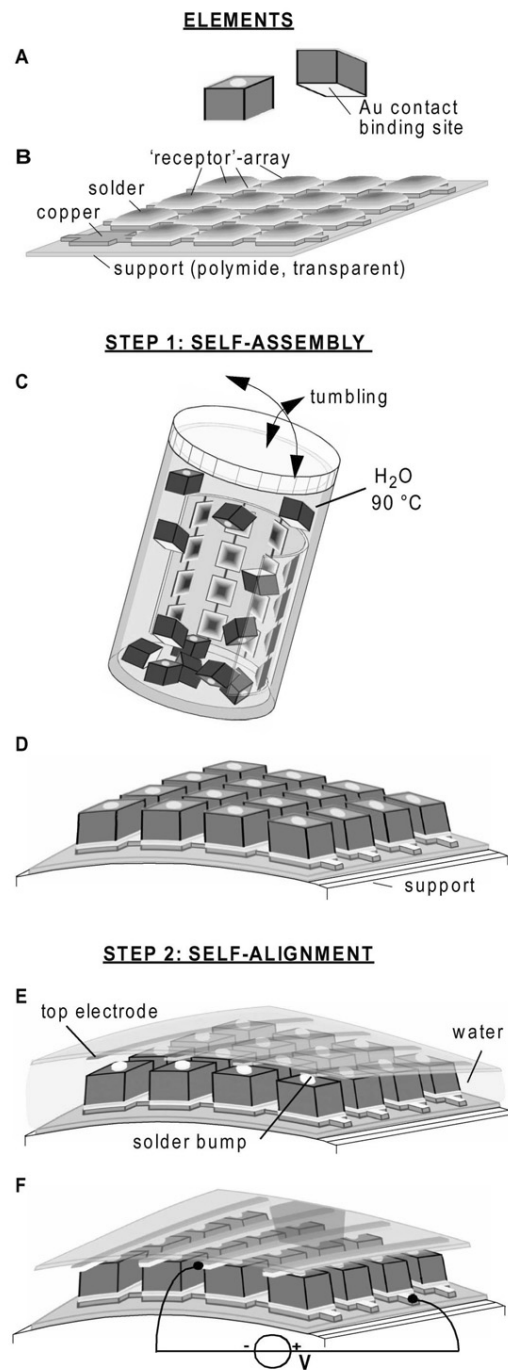


Figure 9 : Procedure used to self-assemble a functional cylindrical display on plastic. (A) Top and bottom views of a LED segment that has two contacts: a small circular Au contact (cathode) on the front, and a large square Au contact (anode) on the back. (B) Array of alloy-coated copper squares supported on a flexible substrate; these squares are the same size as the anodes of the LEDs and act as receptors for the LEDs during the self-assembly. (C) The components are tumbled in a vial at a temperature above the melting point of the alloy. (D) Two-dimensional array of the assembled LEDs. (E) Alignment of a top electrode: The copper wires of the top electrode and the cathodic contacts on the front of the LEDs were first dip-coated with alloy. The array of wires is pre aligned with the array of cathodic alloy bumps. At a temperature above the melting point, electrical connections form and the structure self-aligns. (F) Test of the self-assembled display-prototype [Jacobs et al. (2002)].

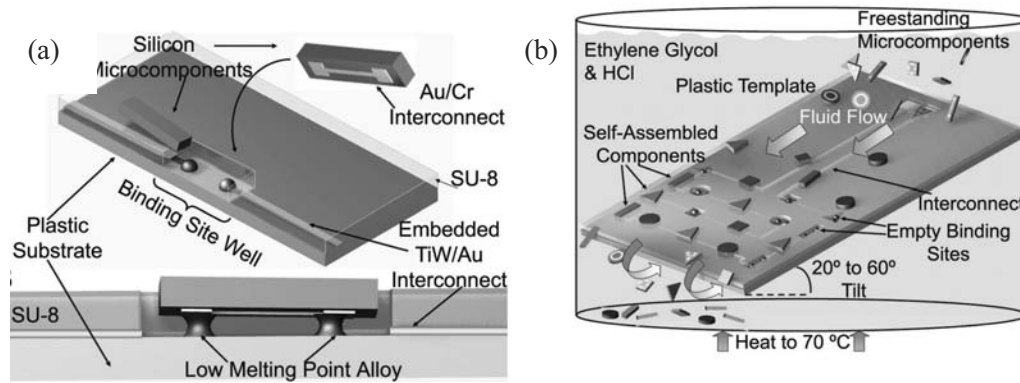


Figure 10 : Illustration of self-assembly process. Microfabricated silicon components assemble at complementary shaped binding sites on the plastic substrate. a) Side view and top view of substrate with components. Low melting point alloy establishes both electrical connection and binding force between part and substrate. b) Fluidic self-assembly process. Substrate is tilted to angle between 20 and 60 degrees and immersed in a solution heated to 70 ° [Stauth and Parviz (2006)].

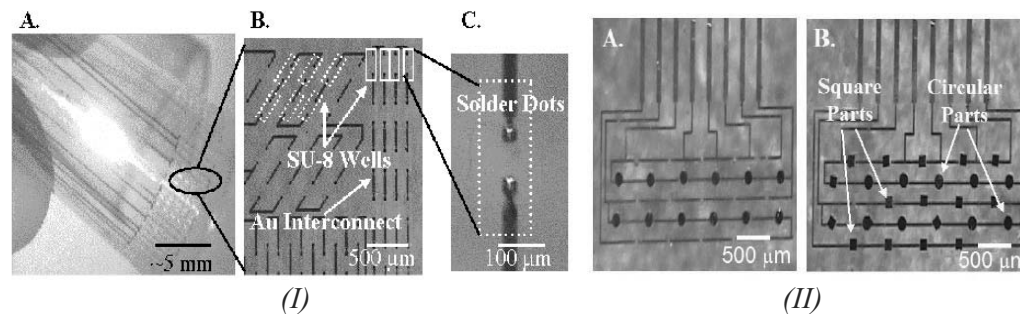


Figure 11 : (I) A) Polyester substrate with binding sites and embedded interconnects. B) Close-up of binding sites; select SU-8 wells are outlined for clarity. C) Binding site and molten alloy. (II) A) Polyester substrate with two types of binding sites. Circular components have assembled into the sites with complementary shapes. B) The self-assembly process continues by the placement of square-shaped parts in the binding sites with matching shapes [Stauth and Parviz (2005) a].

sultant from molten alloy contact between the metal pads on the LEDs and the binding sites trapped the components on the correct location. After arrangement of LEDs on the binding sites, the gold contacts on top of the LEDs were wetted with alloy by dipping the assembly again into a molten alloy bath. The flexible top electrode was manually positioned at an approximately correct position to make contact with the top surface of LEDs. Consequently, the entire structure was heated above the melting point of the alloy to self-align the top electrode. Fig. 9 shows the summary of the process. The process reached ~98% coverage of patterned solder drops in less than 3 minutes for 1500 receptor sites for silicon cubes.

We [Stauth and Parviz (2005) a, Stauth and Parviz (2005) b, Stauth and Parviz (2006)] have demonstrated the FSA

of microfabricated single crystal silicon parts (diffusion resistors and field effect transistors) onto flexible plastic substrates driven in part by capillary forces resultant from low melting point alloy reflow (Fig. 10 and Fig. 11). The self-assembly process done on substrates each containing 10,000 binding sites, realized 97% self-assembly yield within 25 min for 100 μm elements. The advantage of this work compared with the previously mentioned demonstrations is the completion of the self-assembly process in a single step. In this approach all the mechanical and electrical contacts are formed at once and no further processing of the template is necessary. The self-assembly process relies on shape recognition to program the landing sites of the microcomponents on the template. At the bottom of each binding site on the tem-

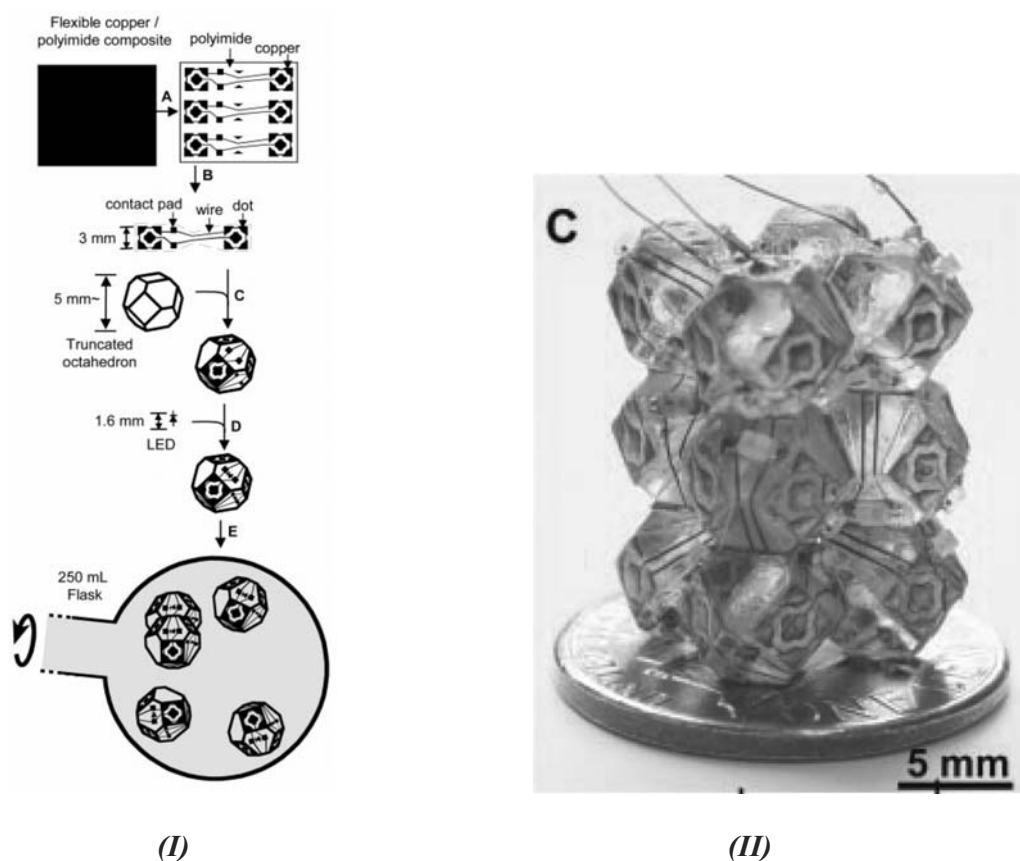


Figure 12 : (I) The procedure used to form electrical networks in 3D by self-assembly: (A) An array of the basic pattern of copper dots, contact pads, and wires was defined on a flexible copper-polyimide sheet using photolithography and etching. (B) These pattern elements were cut out along the dotted line, (C) glued on the faces of the TO, and (D) LEDs were soldered manually onto the contact pads. (E) The copper dots and wires on the TOs were coated with solder, and self-assembly occurred in hot, isodense, aqueous KBr solution [Gracias et al. (2000)] (II) Assembled TOs with biased LEDs emitting red light on them.

plate an area covered by a low melting point alloy is positioned. To perform the self-assembly, the element is submerged in a heated fluid environment. The elevated temperature melts the alloy. The pH of the solution is adjusted to remove the surface oxide from the molten alloy areas. A collection of microcomponents is then introduced into the self-assembly vessel. Controlled vibration of the vessel, gravity, and fluid flow affect the motion of the microcomponents in the fluidic environment. As the shapes of a microcomponent and the corresponding binding site on the template match, the microcomponent enters the binding site allowing the molten alloy to make contact with gold pads positioned on its surface. The resultant capillary force traps the microcomponent in the right location. After all the binding sites are occupied with the appropriate microcomponents, the temperature of

the fluid is lowered to solidify the alloy and make the electrical and mechanical connections permanent.

7 3D Self-Assembly of Freestanding Components

The use of a 2D template can guide the self-assembly process and produce structures with a high yield. Integration of independently fabricated microcomponents into 3D structures is one of the areas in which self-assembly is clearly superior to conventional manufacturing techniques [Benkart et al. (2005)]. A demonstration of this concept with meso-scale components has shown how molten-alloy driven self-assembly can be employed to put a 3D structure together and form electrical connections [Gracias et al. (2000)]. Here, polymer truncated octahedrons (TO) incorporating LEDs were used

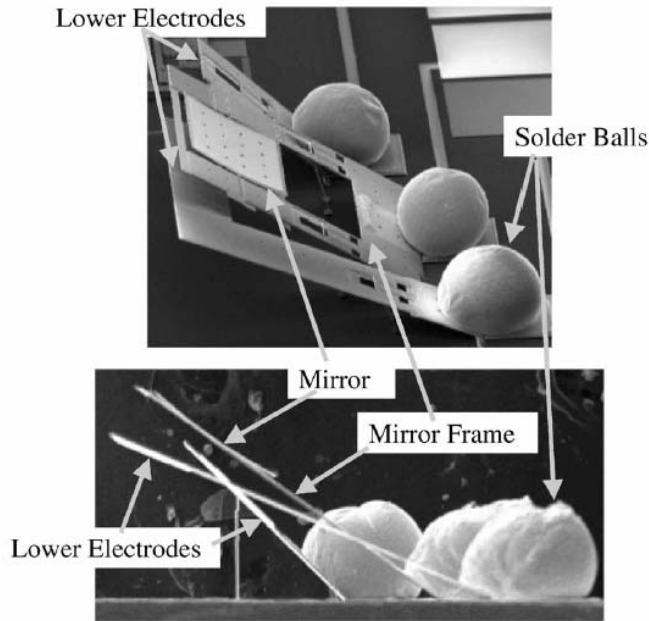


Figure 13 : Scanning electron micrographs of assembled micromirrors [McCarthy et al. (2003) a]. The mirrors fold into their final position, out of the microfabrication plane, as a result of energy minimization of solder balls.

as building blocks. The LEDs were manually wired to patterns of solder dots on adjacent faces of each TO. The TOs were suspended in an isodense liquid at a temperature above the melting point of the solder, and allowed to tumble gently into contact with one another. The drops of molten solder fused, and the minimization of their interfacial free energy generated the forces that assembled the TOs into regular structures (Fig. 12).

The solder pattern on TO faces and procedure of soldering and assembly is shown in Fig. 10. As can be seen in the Figure, patterns were symmetric in all directions. The width of solder dots was about 1 mm, and the optimum distance between adjacent solder dots was one-half of the width. When the patterned TOs were dipped in solder, the wires were also covered with a solder layer. These wires had been made substantially narrower (150 μm), which made the height of solder on them 15 % of that of solder dots. This reduction was necessary because when solder dots fused into connections, wires did not touch and so there was no need for insulating wires to prevent shorting. This work is the first demonstration of using self-assembly for construction of an electrically interconnected 3D structure from independent components.

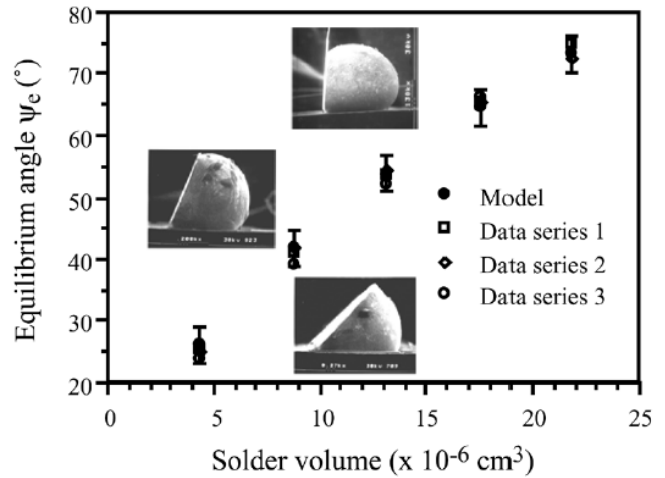


Figure 14 : Comparison between model prediction of equilibrium angle and measured final angles. Error bars represent uncertainty due to solder volume variation [Harsh et al. (2000)].

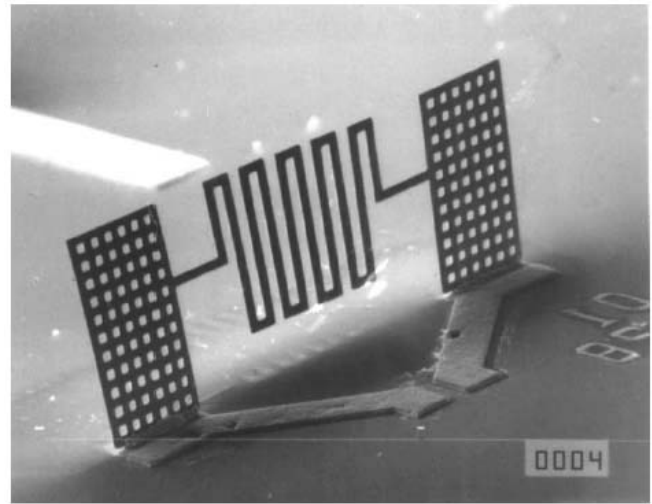


Figure 15 : 4.5-turn meander inductors after self-assembly [Dahlmann et al. (2001)].

8 Molten-Alloy Driven Folding and Positioning

As mentioned above, capillary forces resultant from molten-alloys allow for construction of 3D structures via self-assembly of released and freestanding components. Another application of these capillary forces is to fold or align a partially released microstructure. This type of molten-alloy driven motion has been extensively used in making 3D microelectromechanical systems (MEMS) and in aligning photonic components. In a typical fold-

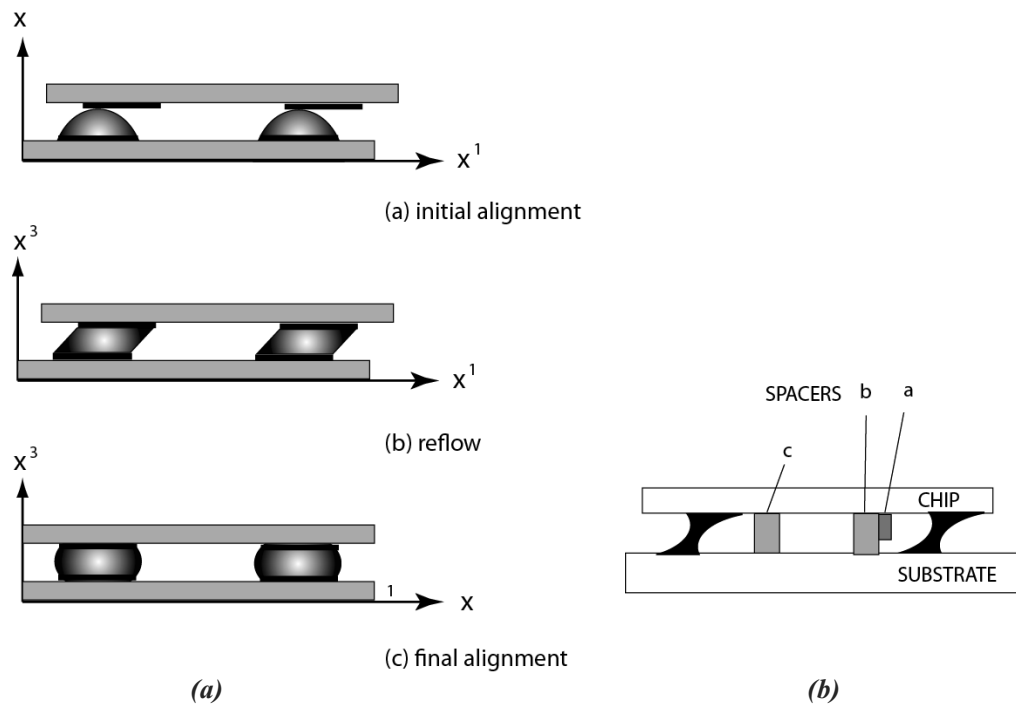


Figure 16 : (a) Self-aligned assembly using solder. (b) Self-aligned assembly using solder and mechanical stop [Lee (1994)].

ing application, a known volume of alloy is positioned on a hinge, bridging between two sections with at least one of the sections free to move. Reflow of the alloy redefines the shape of the metal and drives the system towards a minimum energy state. As the alloy reflows, it causes the motion of the movable part of the microstructure. The final configuration of the hinge, corresponding to a minimum energy state for the alloy, often presents a section of the microstructure folded out of the microfabrication plane on the wafer surface. This approach has been successfully implemented for making micro mirror arrays and for rotating mirrors to different angles [McCarthy et al. (2003) a, McCarthy et al. (2003) b, Harsh et al. (1999)] (Fig. 13).

Given a known quantity of alloy, the motion of the mirrors can be accurately predicted by modeling the surface tension forces. Fig. 14 shows a comparison of surface energy based model predictions and experimental data [Harsh et al. (2000)].

Solder surface tension self-assembly has been used to make high-Q inductors [Dahlmann et al. (2001)] as shown in Fig. 15. By rotating the coil into a plane perpendicular to the substrate, further reduction of capacitance and inductive substrate coupling is achieved. Al-

though this type of self-assembly by folding does not generate arbitrary 3D structures, the out of plane devices and the 2.5D structures yielded extend the utility of conventional microfabrication techniques as seen in the above examples.

Molten-alloy driven motion has been extensively used for precision-aligned optoelectronic assemblies [Xiong et al. (2003), Kallmayer et al. (1996), Sasaki et al. (2001), Lee (1994), Sasaki et al. (1995), Docoslis and Alexandridis (2002)]. Two representative configurations for such assemblies are shown in Fig. 16. In Fig. 16 (a) the top surface is roughly aligned with the solder bumps and the reflow is used to complete the alignment. Despite successful implementation of this procedure, it becomes exceedingly difficult to use this approach for sub-micron level alignment. One of the main reasons for this shortcoming is the loss of capillary force as the alignment makes progress towards the final correct configuration-the full overlap of identical pads generates zero net force parallel to the plane of the pads. One method to remedy this shortcoming is to incorporate mechanical stops, as shown in Fig. 16 (b) to improve the self-alignment process accuracy. Currently, alignment precision of a few hundred nanometers is readily achieved with the approach.

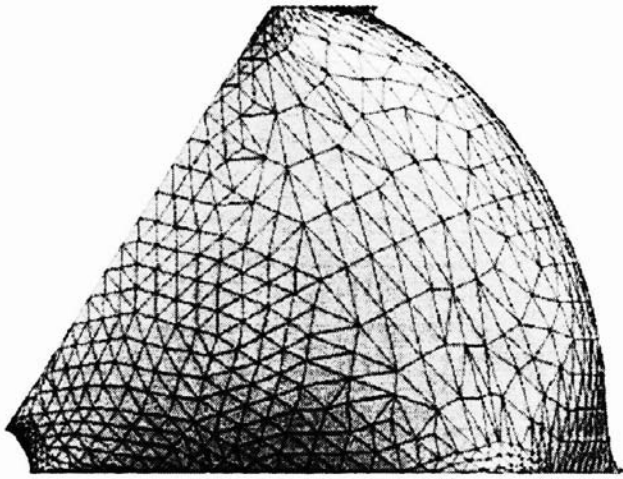


Figure 17 : Stable solder shape with minimum surface energy between two planes with fixed angles as determined by Surface Evolver [Harsh and Lee (1998)].

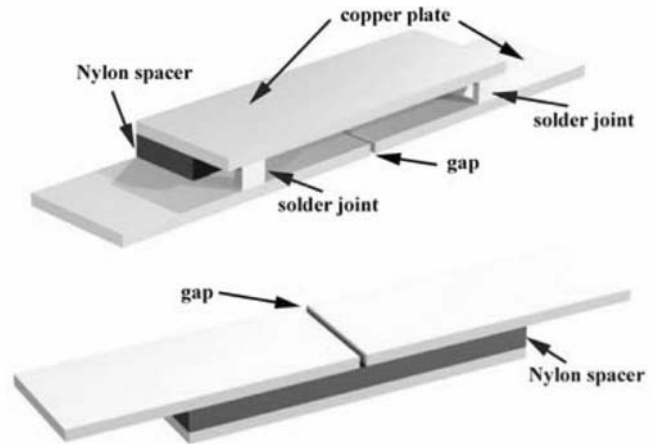


Figure 19 : Experimental set-up for verification of electromigration induced strain simulation results [Ye et al. (2005)].

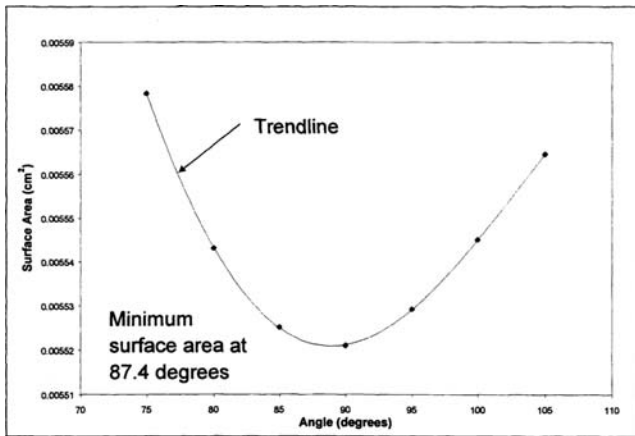


Figure 18 : Surface area (a measure of energy) as a function of angles [Harsh and Lee (1998)].

9 Modeling and Simulation of Alloys

There are a number of different methods and softwares available to model and simulate solder behavior including the modified embedded atom method (MEAM), molecular dynamics (MD) simulation [Dong et al. (2005)], equivalent layer models [Gu 2005], and surface energy minimization modeling [Harsh and Lee (1998)]. Determination of the final shape of a self-assembled alloy structure and its current carrying capacity are of utmost importance in design and integration of heterogeneous systems. Surface energy minimization has been the dominant method used to calculate the fi-

nal shape of a molten alloy after the completion of the self-assembly process. This method can predict the final shape of 3D MEMS configurations and the acting forces, given known geometries, surface energies, and alloy volumes. A number of studies have experimentally validated the results of this type of modeling. For example in [Harsh and Lee (1998)] the experimental results were compared with model predictions for a two-plate pop-up MEMS structure. The experiment confirmed that the model could predict the final, equilibrium angle between the plates to within ± 2 degrees. This and many other works in the field use a freely available modeling software, the Surface Evolver, to calculate the local minimum energy state (Fig. 17). Here, for a given angle between the plates, the total energy of the system was calculated and the solder was allowed to relax to its minimum energy state (Fig. 17). For a constant contact area between the solder and the metal pads, the surface area of the solder is a direct measure of the energy of the configuration. The angle between the plates can be varied and at each angle, the solder can be allowed to relax to its minimum energy state and the total surface area of the solder determined. A plot showing the surface area vs. each angle is shown in Fig. 18. The stable final angle can be identified from the minimum point in this Figure. Although this calculation takes only a few minutes for a simple shape, for complicated geometries, it presents a heavy computational burden. Another issue in setting up the proper initial conditions for such a simulation is

determination of the correct boundary conditions and access to the relevant contact angle and surface energy values.

Electromigration is the transport of material caused by the gradual movement of the ions in a conductor due to the momentum transfer between conducting electrons and diffusing metal atoms. This effect causes solder joints to deform under high current density, which is a commonly encountered issue in small scales. Electromigration effects and consequences can be modeled and simulated with finite element methods (FEM). For example, the structure shown in Fig. 19 has been tested for electromigration induced deformation of solder zones, and has also been simulated using FlexPDE [Ye et al. (2005)].

In this experiment, the current density was close to 1.12×10^4 A/cm², and the height, width, and thickness of the solder were 1.5 mm, 1 mm, and 0.25 mm respectively. The lead-free solder alloy was Sn95.5/Ag4/Cu0.5 with the melting point of 218 °C. The structure was monitored using Moiré interferometry to measure the strain of the solder part as electromigration generated stress. The results of experiment and simulation are shown and compared in Fig. 20. As can be seen in the plots, solder was deformed both in vertical and in horizontal directions as a result of high-density current flow. The experiments show that the deformations created by high current density were significant and irreversible.

10 Scaling and Limits

The smallest solder dots commonly used today are in the order of tens of microns; however, the extension of solder-driven assembly to much smaller scales has also been considered [Harsh et al. (2000)] demonstrating that surface energy minimized solder spheres as small as 5 nm are possible to attain. In a pilot study [Harsh et al. (2000)] 100 nm of pure Indium was evaporated on a silicon wafer and then reflowed at 200 °C for ten minutes to form individual solder dots. Fig. 21 shows the SEM image of the indium spheres on the silicon surface. Unfortunately, the formation of the solder spheres does not immediately translate to a capability to use them in a self-assembly process. A number of significant hurdles remain to be overcome.

IMC formation rapidly consumes nano-scale pads. The new compounds have high melting points, poor surface

tension properties, and can significantly affect the uniformity of the solder at nano-scale and prevent it from forming a capillary bond. Another important parameter is the oxidation rate of the solder especially at higher temperatures necessary to complete a self-assembly process. The oxide thickness can reach tens of nanometers in less than 10 min at 250 °C [Kuhmann et al. (1998)] making the entire alloy volume non-functional. It is evident that a nano-scale molten-alloy driven self-assembly process must be performed under vacuum or inert gas conditions. Since the fluid environment is necessary to allow for random motion of components during the self-assembly process, the only viable option is the saturation of the self-assembly vessel with an inert gas. It should be noted that oxidation is not just a concern at elevated temperatures during the self-assembly process. The formation of the native oxide on a contact formed from many of the alloys mentioned above can readily render a few nanometer contact zone insulating. If the entire contact is only a few nanometers wide, over time, the electrical connectivity will be lost. Such contacts must be protected with thin layers of noble metals such as gold with extremely low oxidation rates.

Various methods can be used to deposit an alloy onto pads used for self-assembly including evaporation, electroplating, and the most commonly used de-wetting. As the size scale of the pads decreases and the solder is forced to deform into larger radius of curvatures to wet the pads, the de-wetting process becomes a less viable option for deposition of the alloys. Also, as it is difficult to generate uniform alloy thickness with de-wetting in nano-scale, it is expected that evaporation and plating will dominate alloy deposition for self-assembly.

11 Conclusions

Self-assembly presents an attractive candidate for integration of heterogeneous multifunctional systems of future both in the micro and in the nano scales. Molten-alloy driven self-assembly, as described here, allows for formation of both mechanical and electrical connections between the components of a system at once and is an attractive approach for system integration. Selection of the appropriate alloy is a critical issue in the design of the self-assembly process. We have catalogued a number of alloys here and identified many that can be potentially used in self-assembly processes. Molten-alloy driven self-assembly has already been extensively used

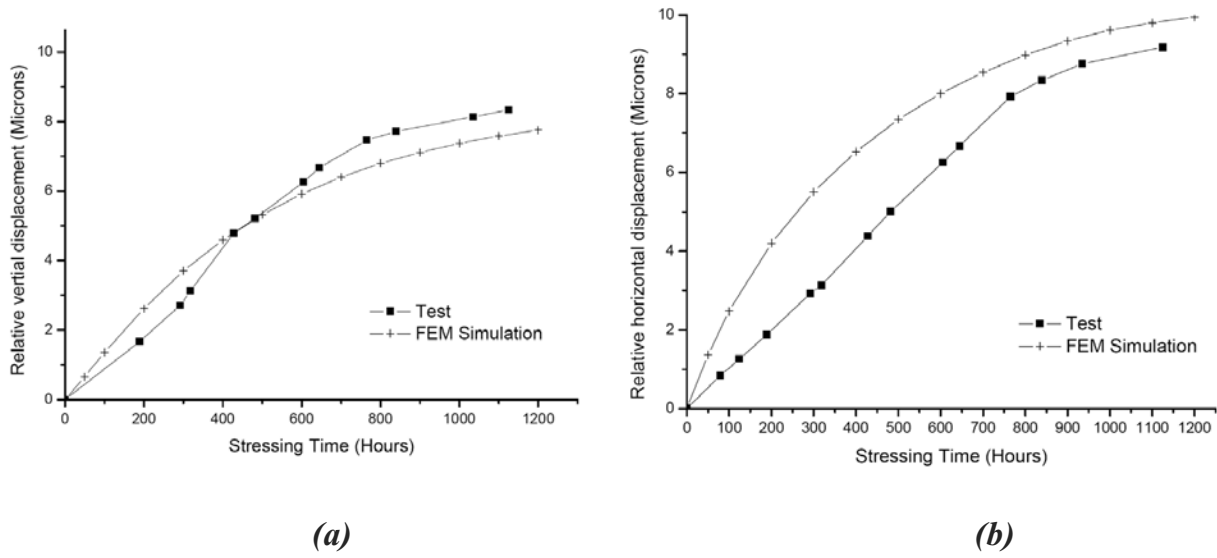


Figure 20 : Comparison between simulation and experimental results of solder displacement caused by electromigration (a) maximum relative vertical displacement between lower and upper interface of solder joint and copper plates (b) maximum relative horizontal displacement between the two edges of the solder joint [Ye et al. (2005)].

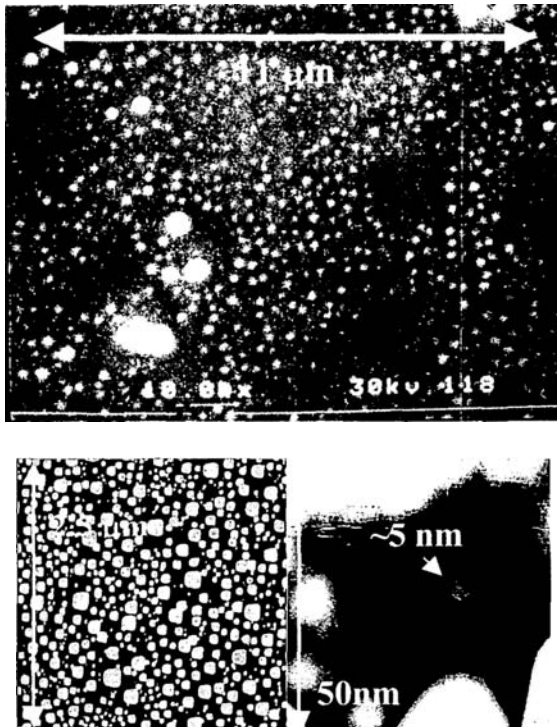


Figure 21 : SEM picture of nano-scale indium solder spheres [Harsh et al. (2000)].

works in the micron-scale have even shown the self-assembly of components onto templates and the self-assembly of released parts into 3D structures for forming integrated systems. Molten-alloy driven self-assembly in the micron scale has made long strides forward and is expected to be heavily used in the next few years for system integrations. A number of issues remain to be addressed in such a system integration scheme including the development of methods to program the self-assembly process, the development of methods to agitate a self-assembling “plasma of parts” and guiding it towards a minimum energy state in the micron-scale, and finally development of modeling methods to predict the outcome of a self-assembly process with high accuracy.

As mentioned above, molten-alloy driven self-assembly has not been demonstrated for the integration of components in the nano-scale. The integration at nano-scale poses major challenges and offers significant opportunities. IMC formation and oxidation are two major issues in nano-scale “soldering”. The surface oxides of the alloys are typically removed in acidic fluxes; the compatibility of the components with these fluxes must be ensured in the self-assembly processes. Many nano-scale components of future may be made from organic materials. Design and synthesis of appropriate organometallic compounds will be critical for developing methods to form high quality electrical contacts to these ob-

in the micron-scale for alignment of optoelectronic components and for folding MEMS structures. Pioneering

jects. In summary, the utility of molten-alloys to drive self-assembly and guide system integration is an untested hypothesis in the nano-scale; however, for system integration needs of near and medium term in the micron-scale, molten-alloy driven self-assembly offers one of the most powerful candidate technologies.

Acknowledgement: The authors thank financial support provided by the National Institutes of Health through grant 5 P50 HG002360 and the Defense Advanced Project Agency through grant # N000140610578. The authors also acknowledge partial support from the National Science Foundation through grant ECS-05-1628.

References

- Abtew, M.; Selvaduray, G.** (2000): Lead-free Solders in Microelectronics. *Materials Science and Engineering*, vol.27, pp. 95-141.
- Artaki, I.; Finely, D.W.; Jackson, A.M.; Ray, U.; Vianco, P.T.** (1995): Wave Soldering with Pb-Free Solders. *Proc. Surface Mount International (San Jose, CA)*, pp. 495.
- Bader, W. G.** (1969): Dissolution of Au, Ag, Pd, Pt, Cu, and Ni in a molten tin-lead solder. *Welding J. Res. Supplement*, vol. 28, no. 12, pp. 551s-557s.
- Benkart, P.; Heittmann, A.; Huebner, H.; Ramacher, U.; Kaiser, A.; Munding, A.; Bschorr, M.; Pfeiderer, H. J.; Kohn, E.** (2005): 3D chip stack technology using throughchip interconnects. *IEEE Design and Test of Computers*, vol. 22, no. 6, pp. 512-518.
- Cohn, M. B.; Böhringer, K. F.; Noworolski, J. M.; Singh, A. ; Keller, C. G. ; Goldberg, K. Y. ; Howe, R. T.** (1998): Microassembly technologies for MEMS. *Proc. SPIE Micromachining and Microfabrication*, (Santa Clara, CA), pp. 2-16.
- Collins, P. G.; Avouris, P.** (2000): Nanotubes for electronics. *Scientific American*, vol. 283.
- Colvin, V.; Schlamp, M.; Alivisatos, A.** (1994): Light emitting diodes made from cadmium selenide nanocrystals and a semiconducting polymer. *Nature*, vol. 370.
- Dahlmann, G.; Yeatman, E.; Young, P.; Robertson, I.; Lucyszyn, S.** (2001): MEMS high q microwave inductors using solder surface tension self-assembly. *IEEE MTT-S International Microwave Symposium Digest*, vol. 1, pp. 229-332.
- de kluzenaar, E.** (1983): Surface oxidation of molten soft solder: An auger study. *J. Vac. Sci. Technol.A*, vol. 1, no. 3, pp. 1480-1485.
- de Gennes, P. G.** (1985): Wetting: statics and dynamics. *Rev. Mod. Phys.*, vol. 57, pp. 827.
- Docoslis, A.; Alexandridis, P.** (2002): One-, two-, and three-dimensional organization of colloidal particles using nonuniform alternating current electric fields. *Electrophoresis*, vol. 23, pp. 2174-2183.
- Dong, H.; Fan, L.; Moon, K.; Wong, C.; Baskes, M.** (2005): Meam molecular dynamics study of lead free solder for electronic packaging applications. *Modelling Simul. Mater. Sci. Eng.*, vol. 13, pp. 1279-1290.
- Dytrych, N. M.** (1993): Reviewing the basics of mass reflow soldering. *Electronic Packaging and Production*, vol. 33, no. 7.
- Erinc, M.; Schreurs, P.; Zhang, G.; Driel, W.; Geers, M.** (2004): Microstructural and mechanical characterization of 95.5sn-4ag-0.scu solder balls by nano-indentation. *5th. Int. Con. on Thermal and Mechanical Simulation and Experiments in Micro-electronics and Micro-Systems*, pp. 443-448.
- Evoy, S.; DiLello, N.; Deshpande, V.; Narayanan, A.; Liu, H.; Riegelman, M.; Martin, B.; Hailer, B.; Bradley, J. C.; Weiss, W.; Mayer, T. S.; Gogotsi, Y.; Bau, H. H.; Mallouk, T.; Raman, S.** (2004): Dielectrophoretic assembly and integration of nanowire devices with functional CMOS operating circuitry. *Microelectron. Eng.*, vol. 75, pp. 31-42.
- Fuhrer, M. S.; Nygrd, J.; Shih, L.; Forero, M.; Yoon, Y. G.; Mazzoni, M. S. C.; Choi, H. J.; Ihm, J.; Louie, S. G.; Zettl, A.; McEuen, P. L.** (2000): Crossed nanotube junctions. *Science*, vol. 288, pp. 494-497.
- Gao, Y. X.; Fan, H.; Xiao, Z.** (2000): A thermodynamic model for solder profile evolution. *Acta mater.* vol. 48, pp. 863-874.
- Gracias, D. H.; Tien, J.; Breen, T. L.; Hsu, C.; Whitesides, G. M.** (2000): Forming electrical networks in three dimensions by self-assembly. *Science*, vol. 289, pp. 3824-3827.
- Gu, J.; Lim, C.; Tay, A.** (2005): Simulation of mechanical response of solder joints under drop impact using equivalent layer models. *Electronic Components and Technology Conference*, pp. 491-498.
- Haiss, W. R.; Nichols, J.; Higgins, S. J.; Bethell,**

- D.; Hobenreich, H.; Schiffrin, D. J.** (2004): Wiring nanoparticles with redox molecules. *Faraday Discuss.*, vol. 125, pp. 179–194.
- Harsh, K. F.; Bright, V. M.; Lee, Y. C.** (2000): Study of micro-scale limits of solder self-assembly for MEMS. *Electronic Components and Technology Conference*, pp. 1690–1695.
- Harsh, K. F.; Bright, V. M.; Lee, Y.** (1999): Solder self-assembly for three-dimensional microelectromechanical systems. *Sensors and Actuators*, vol. 77, pp. 237–24.
- Harsh, K.; Lee, Y. C.** (1998): Modeling for solder self-assembled MEMS. *ISPIE*, vol. 3289, pp. 177–184.
- Hessler, W.** (1996): How to build simple, effective pick-and-place device. *Robotics Today*, vol. 9, no. 4, pp. 1–5.
- Holmes, A. S.; Saidam, S. M.** (1996): Sacrificial layer process with laser-driven release for batch assembly operations. *J. Microelectromech. Syst.*, vol. 7, no. 4, pp. 416–422.
- Hua, F.; Mei, Z.; Glazer, J.** (1998): Eutectic Sn-Bi as an alternative to Pb free solders. *Electronic Components and Technology Conference*.
- Huynh, Q. T.; Liu, C. Y.; Chen, C.; Tu, K. N.** (2001): Electromigration in eutectic SnPb solder lines. *J. Appl. Phys.*, vol. 89, pp. 4332–4335.
- Ishii T.; Aoyama, S.** (2004): Novel micro-bump fabrication for flip-chip bonding. *Journal of Electronic Materials*, vol. 33, no. 11.
- Jacobs, H. O.; Tao, A. R.; Schwartz, A.; Gracias, D. H.; M. Whitesides, G.** (2002): Fabrication of a cylindrical display by patterned assembly. *Science*, vol. 296, pp. 323–325.
- Kallmayer, C.; Oppermann, H.; Eugelmann, G.; Zankel, E.; Reichl, H.** (1996): Self-aligning flip-chip assembly using eutectic gold/tin solder in different atmospheres. *Nineteenth IEEE/CPMT Electronics Manufacturing Technology Symposium*, pp. 18–25.
- Kang, S. C.; Kim, C.; Muncy, J.; Baldwin, D.F.** (2005): Experimental wetting dynamics study of eutectic and lead-free solders with various fluxes, isothermal conditions, and bond pad metallizations. *IEEE Transactions on Advanced Packaging*, vol. 28, no. 3, pp. 465–74.
- Kim, H.; Liou, H.; Tu, K.** (1995): Three-dimensional morphology of a very rough interface formed in the soldering reaction between eutectic SnPb and Cu. *Appl. Phys. Lett.*, vol. 66, pp. 2337–2339.
- Kim, H.; Tu, K.** (1996): Kinetic analysis of the soldering reaction between eutectic snpb alloy and cu accompanied by ripening. *Phys. Rev. B*, vol. 53, pp. 16027–16034.
- Kuhmann, J. F.; Preuss, A.; Adolphi, B.; Maly, K.; Wirth, T.; Oesterle, W.; Pittroff, W.; Weyer, G.; Fanciulli, M.** (1998): Oxidation and reduction kinetics of eutectic SnPb, InSn, and AuSn: A knowledge base for fluxless solder bonding applications. *IEEE Transactions on Components, Packaging, and Manufacturing Technology- Part C*, vol. 21, no. 2, pp. 134–140.
- Lee, K.; Choi, J.; Janes, D. B.** (2004): Measurement of I-V characteristic of organic molecules using step junction. *4th IEEE Conference on Nanotechnology*.
- Lee, Y. C.** (1994): Studies on solder self-alignment. *IEEE Lasers and Electro-Optics Society 7th Annual Meeting*, vol. 1, no. 1, pp. 73–74.
- Li, Y.; Wong, C.P.** (2006): Recent advances of conductive adhesives as a lead-free alternative in electronic packaging: Materials, processing, reliability and applications. *Materials Science and Engineering*, vol. 51, pp. 1–35.
- Madsen, D.; Molhave, K.; Mateiu, R.; Boggild, P.; Rasmussen, A.; Appel, C.; Brorson, M.; Jacobsen, C.** (2003): Nanoscale soldering of positioned carbon nanotubes using highly conductive electron beam induced gold deposition. *Third IEEE Conference on Nanotechnology*, pp. 12–14.
- Mallicka, K.; Witcomb, M. J.; Scurrilla, M. S.** (2005): Selfassembly of silver nanoparticles in a polymer solvent: formation of a nanochain through nanoscale soldering. *Materials Chemistry and Physics*, vol. 90, pp. 221–224.
- McCarthy, B.; Bright, V. M.; Neff, J. A.** (2003 a): A multicomponent solder self-assembled micromirror. *Sensors and Actuators A*, vol. 103, pp. 187–193.
- McCarthy, B.; Bright, V. M.; Neff, J. A.** (2003 b): A solder self-assembled torsional micromirror array. *The Sixteenth Annual International Conference on Micro Electro Mechanical Systems, (Kyoto)*, pp. 215–218.
- McCreery, R. L.** (2004): Molecular electronic junctions. *Chem. Mater.*, vol. 16, pp. 4477–4496.
- Miric, A.Z.; Grusd, A.** (1998): Lead-free alloys. *Soldering & Surface Mount Technology*, vol. 10, no. 1, pp. 19–25.
- Morris, C.J.; Stauth, S.A.; Parviz, B.A.** (2005): Self-

- Assembly for Microscale and Nanoscale Packaging: Steps toward Self-Packaging. *IEEE Transactions on Advanced Packaging*, vol. 28, no. 4, pp 600-11.
- Nah, J. W.; Ren, F.; Tu, K. N.; Venk, S.; Camara, G.** (2006): Electromigration in Pb-free flip chip solder joints on flexible substrates. *Journal of Applied Physics*, vol. 99, pp. 023520.
- Odom, T. W.; Huang, J. L.; Kim, P.; Lieber, C. M.** (1998): Atomic structure and electronic properties of single-walled carbon nanotubes. *Nature*, vol. 391, pp. 62–64.
- Parviz, B. A.; Ryan, D.; Whitesides, G. M.** (2005): Using self-assembly for the fabrication of nano-scale electronic and photonic devices. *Ann. Rev. Fluid Mech.*, vol. 37, pp. 425–455.
- Renken, F.P.; Subbarayan, G.** (1998): A two-body formulation for solder joint shape prediction. *Transactions of the ASME. Journal of Electronic Packaging*, vol. 120, no. 3, pp. 302-8.
- Saito, R.; Fujita, M.; Dresselhaus, G.; Dresselhaus, M. S.** (1992): Electronic structure of chiral graphene tubules. *Appl. Phys. Lett.*, vol. 60, pp. 2204–2206.
- Sasaki, J.; Honmou, H.; Itoh, M.; Uda, A.; Torikai, T.** (1995): Self-aligned assembly technology for laser diode modules using stripe-type ausn solder bump flip-chip bonding. *IEEE Lasers and Electro-Optics Society Annual Meeting. 8th Annual Meeting. Conference Proceedings*, vol. 1, no. 1, pp. 234–235.
- Sasaki, J.; Itoh, M.; Tamanuki, T.; Hatakeyama, H.; Kitamura, S.; Shimoda, T.; Kato, T.** (2001): Multiple-chip precise self-aligned assembly for hybrid integrated optical modules using AuSn solder bumps. *IEEE TRANSACTIONS ON ADVANCED PACKAGING*, vol. 24, no. 4, pp. 569–575.
- Seelig, K.; Suraski, D.** (2001): Advanced materials considerations for lead-free electronics assembly. *The International Journal of Microcircuits and Electronic Packaging*, vol. 24, no. 4, pp. 366–378.
- Stauth, S. A.; Parviz, B.A.** (2006): Self-assembled single-crystal silicon circuits on plastic. *PNAS*, vol. 103, pp. 13922-13927.
- Stauth, S. A.; Parviz, B. A.** (2005 a): Self-assembled silicon networks on plastic. *The 13th International Conference on Solid-State Sensors, Actuators and Microsystems*, (Seoul, Korea), pp. 964–967.
- Stauth, S. A.; Parviz, B. A.** (2005 b): Integration of silicon circuit components onto plastic substrates using fluidic self-assembly. *Proceedings of the 2005 International Conference on MEMS, NANO and Smart Systems*.
- Syms, R. R. A.** (2001 a) Measurement of starting torque in surface tension self-assembly of microstructures. *Electron. Lett.*, vol. 37, pp. 859–861.
- Syms, R. R. A.; Gormley, C.; Blackstone, S.** (2001 b): Improving yield, accuracy and complexity in surface tension self-assembled MOEMS. *Sens. Actuators*, vol. 88, no. 3, pp. 273–283.
- Syms, R. R. A.** (2000): Self-assembled 3D silicon microscanners with self-assembled electrostatic drives. *IEEE Photon. Technol. Lett.*, vol. 12, pp.1519–1521.
- Syms, R. R. A.** (1998) Rotational self-assembly of complex microstructures by the surface tension of glass. *Sens. Actuators*, vol. A65, pp. 238–243.
- Syms, R. R. A.** (1999): Surface tension powered self-assembly of 3-D micro-optomechanical structures. *J. Microelectromech. Syst.*, vol. 8, pp. 448–455.
- Syms, R. R. A.; Huang, W.; Schneider, V. M.** (1996): Optimization of borophosphosilicate glass compositions for silica-on-silicon integrated optical circuits fabricated by the sol-gel process. *Electron. Lett.*, vol. 32, pp. 1233–1234.
- Syms, R. R. A.; Yeatman, E.M.; Bright, V.M.; Whiteside, G.M.** (2003): Surface Tension-Powered Self-Assembly of Microstructures—The State-of-the-Art. *Journal of Microelectromechanical systems*, vol.12, no.4, pp. 387-417.
- Talghader, J. J.; Tu, J. K.; Smith, J. S.** (1995): Integration of fluidically self-assembled optoelectronic devices using a silicon-based process. *IEEE Photonics Technology Letters*, vol. 7, no. 11, pp. 1321–1323.
- Tanase, M.; Silevitch, D. M.; Hultgren, A.; Bauer, L. A.; Searson, P. C.; Meyer, G. J.; Reich, D. H.** (2002): Magnetic trapping and self-assembly of multicomponent nanowires. *J. Appl. Phys.*, vol. 91, pp. 8549–8551.
- Technical Reports for the Lead-Free Solder Project: Properties Reports** (1998): Room Temperature Tensile Properties of Lead-Free Solder Alloys. *Lead-Free Solder Project CD-ROM, National Center for Manufacturing Sciences (NCMS)*.
- Tu, K.; Gusak, A.; Li, M.** (2003): Physics and materials challenges for lead-free solders. *Journal of applied*

Physics, vol. 93, no. 3, pp. 1335–1353.

Unruh, K.; Huber, T.; Huber, C. (1993): Melting and freezing behavior of indium metal in porous glasses. *Phys. Rev. B*, vol. 48, pp. 9021–9027.

Wang, H.; Ma, X.; Gao, F.; Qian, Y. (2006): Sn concentration on the reactive wetting of high-Pb solder on Cu substrate. *Materials Chemistry and Physics* 99, pp. 202–205.

Whalley, D.C.; Conway, P.P. (1996): Simulation and interpretation of wetting balance tests using the surface evolver. *Journal of Electronic Packaging, Transactions of the ASME*, vol. 118, no. 3, pp. 134–141.

Wilder, J. W. G.; Venema, L. C.; Rinzler, A. G.; Smalley, R. E.; Dekker, C. (1998): Electronic structure of atomically resolved carbon nanotubes. *Nature*, vol. 391, pp. 59–62.

Xiong, X.; Hanein, Y.; Fang, J.; Wang, W.; Wang, W.; Schwartz, D.T.; Bohringer, K.F. (2003) Controlled multibatch self-assembly of microdevices. *Journal of Microelectromechanical Systems*, vol. 12, no. 2, pp 117 – 127.

Xu, G. (2001): *M.Sc thesis, University of California, Los Angeles.*

Ye, H.; Basaran, C.; Hopkins, D. C.; Lin, M. (2005): Modeling deformation in microelectronics BGA solder joints under high current density, part i: Simulation and testing. *Electronic Components and Technology Conference*, pp. 1437–1444.

Ye, H.; Gu, Z.; Yu, T.; Gracias, D. H. (2006): Integrating nanowires with substrates using directed assembly and nanoscale soldering. *IEEE Transactions on nanotechnology*, vol. 5, pp. 62–66.

Ye, H.; Gu, Z.; Yu, T.; Bernfeld, A.; Leong, T.; Gracias, D. H. (2005): Forming low resistance nano-scale contacts using solder reflow. *Proceedings of 2005 5th IEEE Conference on Nanotechnology*, (Nagoya, Japan).

Yeh, E. C.; Choi, W. J.; Tu, K. N.; Elenius, P.; Balkan, H. (2002): Current-crowding-induced electromigration failure in flip chip solder joints. *Appl. Phys. Lett.*, vol. 80, pp. 580–582.

Yost, F.G.; Sackinger, P.A.; O’Toole, E.J. (1998): Energetics and kinetics of dissolutive wetting processes. *Acta Materialia*, vol. 46, no. 7, pp. 2329–36.

Zheng, W.; Chung, J. B.; Jacobs, H. O. (2005 a): Nonrobotic fabrication of packaged microsystems by

shapeand- solder directed self-assembly. *18th IEEE International Conference on Micro Electro Mechanical Systems*, pp. 8–11.

Zheng, W.; Jacobs, H. O. (2005 b): Fabrication of multicomponent micorsystems by directed three-dimensional selfassembly. *Adv. Funct. Mater.*, vol. 15, no. 5, pp. 732– 738.

Ziegler, J. F.; Srinivasan, G. R. (1996): Terrestrial cosmic rays and soft errors. *IBM J. Res. Dev.*, vol. 40, no. 1.

